Journal of Magnetic Resonance 212 (2011) 254–264

Contents lists available at ScienceDirect

Journal of Magnetic Resonance

journal homepage: www.elsevier.com/locate/jmr

Reduction of magnetic field fluctuations in powered magnets for NMR using inductive measurements and sampled-data feedback control

Mingzhou Li [a], Jeffrey L. Schiano [a,*], Jenna E. Samra [a], Kiran K. Shetty [b], William W. Brey [b]

[a] Pennsylvania State University, Department of Electrical Engineering, University Park, PA 16802, USA
[b] National High Magnetic Field Laboratory, Center for Interdisciplinary Magnetic Resonance, Tallahassee, FL 32310, USA

ARTICLE INFO

Article history:
Received 10 February 2011
Revised 10 May 2011
Available online 7 June 2011

Keywords:
High-field resistive magnet
Hybrid magnet
Temporal magnetic field fluctuations
Feedback control

ABSTRACT

Resistive and hybrid (resistive/superconducting) magnets provide substantially higher magnetic fields than those available in low-temperature superconducting magnets, but their relatively low spatial homogeneity and temporal field fluctuations are unacceptable for high resolution NMR. While several techniques for reducing temporal fluctuations have demonstrated varying degrees of success, this paper restricts attention to methods that utilize inductive measurements and feedback control to actively cancel the temporal fluctuations. In comparison to earlier studies using analog proportional control, this paper shows that shaping the controller frequency response results in significantly higher reductions in temporal fluctuations. Measurements of temporal fluctuation spectra and the frequency response of the instrumentation that cancels the temporal fluctuations guide the controller design. In particular, we describe a sampled-data phase-lead-lag controller that utilizes the internal model principle to selectively attenuate magnetic field fluctuations caused by the power supply ripple. We present a quantitative comparison of the attenuation in temporal fluctuations afforded by the new design and a proportional control design. Metrics for comparison include measurements of the temporal fluctuations using Faraday induction and observations of the effect that the fluctuations have on nuclear resonance measurements.

1. Introduction

Increasing the magnetic field strength B_0 greatly improves several aspects of NMR experiments. It is well known that spectral resolution in NMR increases linearly with field, and sensitivity increases typically as $B_0^{7/4}$, justifying the drive to higher field. Other effects, with even stronger dependence on field, become significant in the 20–36 T range. Resolution in spectra of quadrupolar nuclei has been shown to improve as B_0^2 up to at least 40 T, resulting in new opportunities for the study of many scientifically and commercially important ceramics [1]. The high field increases the effect of intermolecular multiple-quantum coherences (iMQCs) that may be important both as a tool for improving spectral resolution [2,3] and as a new mechanism for image contrast [4].

Magnets with fields of 40 T and above are presently available to the research community, but the field quality of these magnets is not adequate for most NMR experiments. In addition to a high field strength, NMR experiments generally also require both a high spatial field homogeneity and small temporal field fluctuations. In addition to distorting the phase and broadening the NMR line, temporal field fluctuations reduce the effectiveness of coherent signal averaging [5] and disturb the phase of the spin echo [2,6]. The focus of this paper is on the characterization and reduction of temporal field fluctuations. Methods for reducing the effect of poor spatial homogeneity, although outside the scope of this paper, may also be required.

For magnets realized with low-temperature superconductors (LTS), high spatial homogeneity and small temporal field fluctuations are readily attained using shims and a field frequency lock. Because physical properties of LTS coils limit the upper field strength to 22 T [7], alternative magnet technologies have been used to achieve higher field strengths. For example, several groups are developing LTS/HTS magnets with field strengths in excess of 23 T by surrounding an inner high-temperature superconducting (HTS) coil with an outer LTS coil [8,9]. High field strengths can also be achieved using resistive magnets that operate with either pulsed or continuous power sources. Pulsed resistive magnets have lower installation and operating costs, but suffer from short duration fields characterized by large temporal fluctuations. The use of a pulsed resistive magnet to acquire ^{1}H spectra at 56 T has been demonstrated [10].

Resistive and hybrid resistive/superconducting magnets using continuous power sources produce fields up to 45 T, approximately twice that of available superconductive magnets used for NMR [11]. However, their relatively low homogeneity and high level of field ripple and drift, as well as their high operating cost, have to

* Corresponding author. Fax: +1 814 863 5341.
E-mail address: schiano@psu.edu (J.L. Schiano).

1090-7807/$ - see front matter © 2011 Published by Elsevier Inc.
doi:10.1016/j.jmr.2011.05.010

date limited the application of these magnets for NMR [12]. The National High Magnetic Field Laboratory is presently constructing a hybrid resistive/superconducting magnet designed to produce a field of up to 36 T at higher homogeneity and lower ripple than has previously been possible [13,14]. While it will not have as high a field as the world record 45 T hybrid [11], the new magnet will have a lower operating cost and the 40 mm bore is appropriate for NMR probes. Field homogeneity will be improved by the presence of high-strength resistive shim coils integrated into the magnet [15]. Unlike the 45 T magnet, the resistive and superconductive windings will be operated in series mode from a single power supply. Because of this fact, the magnet is known as the series-connected hybrid (SCH).

An advantage of the SCH design is that the series mode increases the magnet's time constant by a factor of more than 20, thereby reducing temporal field fluctuations. Even with its high inductance, the field of the SCH will be subject to fluctuations from the power supply and water cooling system that will adversely affect the NMR signal. The NHMFL power supply system has been designed to minimize these fluctuations. Passive and active power supply filters reduce the peak-to-peak current ripple to about 3 ppm over a period of a few minutes [16]. Water temperature regulation is also important. For a resistive magnet, the sensitivity of magnetic field strength to temperature fluctuations was found by NMR to be about 17 ± 1 ppm/°C. Improvements in the design of the water cooling system reduced the peak-to-peak variation in water temperature over a period of minutes to 0.15 °C, resulting in field fluctuation of 2.5 ppm [17]. Further NMR measurements found a total peak-to-peak field variation of about 5 ppm.

When this 36 T series-connected hybrid magnet is completed it will provide a unique window into magnetic resonance phenomena at high field. Also, because the SCH can easily be ramped from one field to another, it will be well-suited to measurements of field-dependent relaxation and for the investigation of extremely broad lines. The magnet will be operated as a user facility, available to scientists throughout the world. Its unique capabilities are expected to support a thriving user program in magnetic resonance.

With the exception of persistent-mode LTS magnets, all of the aforementioned magnet technologies require an external power source. As a consequence of Ampere's law, inevitable supply current ripple produces undesirable temporal fluctuations in the field strength. A number of different approaches have been applied to correcting field fluctuations in magnets. These include passive suppression, post processing, and experiments that are intrinsically insensitive to field fluctuations.

Passive suppression techniques surround the sample with a shield consisting of a highly conductive material [19,20]. The temporal magnetic field fluctuations induce eddy currents within the shield. By Lenz's law, these currents generate a magnetic field that opposes the fluctuations. Using a helium cooled shield, Sigmund reported a 20-fold decrease in the 60 Hz component of the magnetic field fluctuations to a residual level of about 0.1 ppm [20].

Another strategy is to correct the NMR signal based on an independent record of the temporal magnetic field fluctuations. An appropriate deconvolution algorithm can be used to correct the signal by postprocessing, which must of course be done prior to signal averaging [21]. The reference signal may be conveniently derived from an inductive pickup coil placed close to the NMR sample [22,23]. For experiments that require a greater degree of correction, a technique known as HEteroNuclear PhasE Corrected (HENPEC) spectroscopy has been proposed [24]. The reference for HENPEC is derived from the NMR signal of the deuterated liquid into which the sample has been dissolved. In conjunction with magic angle spinning, HENPEC has allowed the measurement of linewidths as small as 0.04 ppm to be observed in resistive magnets. Deconvolution has also been used to reduce the effect of a changing B_0 for NMR in a pulsed magnet [10].

A third strategy is to use a pulse sequence whose response is insensitive to temporal fluctuations yet preserves chemical shift and J couplings. One proposed experiment, HOMOGENIZED-CPMG, allows for high resolution NMR in the presence of both field inhomogeneity and moderate temporal fluctuations [2]. It encodes the spectral information as intermolecular zero-quantum coherences (iZQC) that are read out through a multiple-echo sequence. Using this technique, Lin et al. measured linewidths of about 0.02 ppm in a sample of water and acetone. Preliminary heteronuclear 2D spectra have been recorded using another approach, the ultrafast single-scan 2D experiment [6]. These experiments rely on capturing the entire spectral dataset within 5–10 ms, obviating the need for stability on a longer term basis. Sub-ppm spectra were recorded from a 5 mm NMR tube in spite of the background fluctuations. A related technique was recently proposed by Pelupessy et al. [25].

This paper considers a fourth strategy, in which the temporal fluctuations are reduced using feedback control. This technique requires a sensor for observing the magnetic field fluctuations, a compensator, and a correction coil driven by a current amplifier. The magnetic field fluctuations are detected by a sensor, in this case a pickup coil. The correction coil superimposes a magnetic field that suppresses the magnetic field fluctuations. The compensator couples the magnetic field sensor to the current amplifier input, and its design determines the frequency-dependent reduction in the temporal magnetic field amplitude.

In the late 1950s, Gunthard and Primas first demonstrated a feedback control system which used inductive measurements to reduce the amplitude of low frequency magnetic field fluctuations in permanent magnets [26,27]. Twenty years later, Gottlieb et al. described a similar approach to attenuate temporal magnetic fluctuations in a Bitter-type resistive magnet [28]. Feedback systems using inductive sensors are well suited to reduce power supply ripple and other fluctuations having a relatively high frequency. The lower limit of their useful frequency range results from 1/f noise and the fact that the induced voltage in the coil is proportional to the frequency of the field fluctuations.

An alternative, and often complimentary method for measuring and regulating the magnetic field is to observe the NMR signal of a reference sample. Packard demonstrated the use of NMR measurements to sense and correct variations in the static magnetic field in 1948 [29]. This method, which is called a field-frequency lock, is widely used in NMR instrumentation [30]. Field-frequency locks require that the magnetic field varies slowly in comparison to the RF pulse rate, and are less effective at removing high frequency fluctuations that arise from power supply harmonics in resistive magnets. They are widely used to reduce drift in superconductive NMR magnets. Resistive magnets can benefit from employing both inductive feedback control and a field-frequency lock to reduce field fluctuations from zero to several hundred Hz [17].

Feedback control designs for reducing magnetic field fluctuations have typically employed simple compensators whose behavior could be represented by a first or second order differential equation, such as the proportional plus integral plus derivative (PID) compensator [18]. These controllers are reasonable to implement with analog components, and it is relatively straightforward to manually adjust the controller gains through trial and error. However, simple controllers can provide only a modest level of fluctuation suppression. Higher-order control designs are well known, and while it may not be practical to implement them with analog components, it is possible to realize the required functions using digital signal processing equipment. Determination of the correct parameters typically requires a dynamic model of the process to be controlled. Our hypothesis for this project was that high-

er order control designs might be used to obtain a greater degree of fluctuation suppression in resistive and hybrid resistive-superconductive magnets. We were prepared to employ a DSP-based controller, and to carry out systematic measurements to extract an accurate model of our fluctuation suppression system in order to design the feedback control system.

This paper describes the design of a phase-lead-lag compensator that uses the internal model principle to selectively suppress fluctuations at harmonics of the power supply ripple. This design, denoted as the PLL-IMP compensator, was realized using a dedicated signal processing system controlled through a personal computer. Because the SCH magnet is not yet completed, the flux regulation system was developed and tested using a 25 T, 52 mm bore resistive magnet developed with the support of the Keck foundation [31]. The flux regulator attenuates the 60 Hz component of the field fluctuation by more than 60 dB. Most elements of the flux regulation system will be later implemented on the SCH. In the mean time, NMR users of the Keck magnet will benefit from reduced field fluctuations.

The remaining three sections summarize the design and evaluation of the PLL-IMP compensator. Section 2 describes two metrics for quantifying the reduction in magnetic field fluctuations. Section 3 details the design and implementation of the PLL-IMP compensator. Section 4 compares the reduction in magnetic field fluctuations obtained with a proportional controller and the PLL-IMP compensator for the Keck resistive magnet.

2. Performance metrics

This section describes two metrics for quantifying the effectiveness of a feedback control system in reducing the amplitude of magnetic field fluctuations. One metric is the magnitude spectrum taken from the flux regulation system's inductive sensor. The fluctuation spectrum provides the most direct information about sources of field noise and the performance of the flux regulation algorithm. The second metric is the uncertainty in the phase of the NMR signal as a function of echo time. The echo phase uncertainty gives less information about the field fluctuations, but it more accurately reflects the requirements of the NMR experiments that are performed.

2.1. Inductive measurements

Section 2.1.1 describes how we estimate the magnitude spectra of magnetic field fluctuations using inductive measurements while Section 2.1.2 shows example spectra from the Keck resistive magnet operating at 7.1 T. Section 2.1.3 discusses the disadvantages of using inductive measurements to estimate magnetic field fluctuations, and motivates the use of NMR measurements described in Section 2.2.

2.1.1. Theory

Faraday induction provides a straightforward means for observing magnetic field fluctuations. The open circuit voltage across a solenoidal pickup coil is proportional to the derivative of the temporal fluctuations $B_f(t)$

$$v_{oc}(t) = AN\frac{dB_f(t)}{dt}, \tag{1}$$

where N represents the number of turns of the coil and A is the cross-sectional area of the coil. Integrating the open-circuit voltage provides an estimate of the magnetic field fluctuations $B_f(t)$. A pure integrator is undesirable as small DC offsets in analog instrumentation will saturate the integrator output. Instead, we use an amplifier with transfer function

$$H_{int}(s) \equiv \frac{V_{int}(s)}{V_{oc}(s)} = \frac{K}{s\tau + 1}, \tag{2}$$

where K represents the DC gain and τ is the amplifier time constant. For frequencies greater than $1/\tau$, the amplifier behaves as an integrating preamplifier with transfer function $H_{int}(s) \approx K/s\tau$. The estimate of the magnetic field fluctuation is

$$B_f(t) = \frac{\tau}{K\,A\,N}\,v_{int}(t), \tag{3}$$

where $v_{int}(t)$ is the integrating preamplifier output voltage. From Eq. (3), the magnitude spectrum of $B_f(t)$ is obtained by scaling the magnitude spectrum of $v_{int}(t)$ by KAN/τ.

2.1.2. Inductive measurements

A solenoidal pickup coil is centered within the Keck magnet and consists of 1770 turns of AWG 36 wire wound around a 13.1 mm diameter, 25.4 mm long, quartz tube. The self-resistance and inductance of the pickup coil are approximately 114 Ω and 1.6 mH, respectively. The pick up coil is connected to the input of the integrating preamplifier. The pickup coil impedance and preamplifier input impedance form a first-order lowpass filter that can be neglected because its 3 dB corner frequency of 200 kHz far exceeds the bandwidth of the preamplifier. Furthermore, because the input resistance of the integrating preamplifier is much larger than the self-resistance of the pickup coil, the voltage across the integrating preamplifier input terminals approximates the open circuit voltage of the pickup coil.

The integrating preamplifier has the transfer function representation in Eq. (2), where the time constant τ is 0.4 s and the DC gain K is 100. A dynamic signal analyzer (DSA) records the spectrum of the integrating preamplifier output voltage. The low and high frequency limits of the spectrum are set by the acquisition window length and sampling rate, respectively. The DSA provides the rms signal magnitude at 801 frequency points, ranging from 1 Hz to 1601 Hz in 2 Hz steps. Using Eq. (3), the magnitude spectrum of the magnetic field fluctuation is reported in units of G rms.

Fig. 1 shows a series of typical magnitude spectra of the magnetic field fluctuations observed in the Keck magnet operating at 7.1 T. The four curves in Fig. 1 represent separate observations spanning a two year period. The small magnitude variations between the curves reflect the fact that multiple users present a varying load to the NHMFL power supply system. The salient peaks are located at the 60 Hz harmonics of the power supply output. The largest peak is located at 60 Hz, and has a value of 160 mG rms,

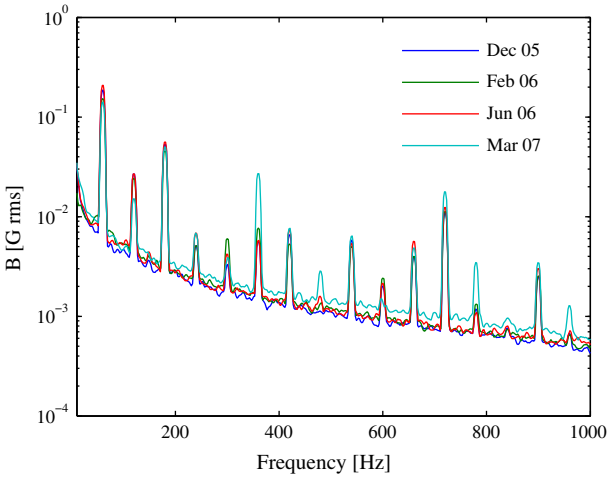

Fig. 1. Magnitude spectra of the temporal magnetic field fluctuations in the Keck resistive magnet operating at 7.1 T.

or equivalently, 2.28 ppm rms. From the standpoint of designing a control system to attenuate the harmonic components, it is important to note that the spectral location of the peaks remains fixed.

2.1.3. Limitations of inductive measurements

While inductive measurements using a pickup coil provide a direct measure of the temporal magnetic field fluctuations, this technique has several limitations. Induction detects only changes in the field, not the field itself, and so it is limited to relatively rapid fluctuations. The signal-to-noise ratio of the estimate provided by Eq. (3) decreases with the frequency of the magnetic field fluctuations because of 1/f noise and the linear dependence of the induced voltage $v_{oc}(t)$ on frequency. For instance, the cooling system produces magnetic field fluctuations with frequency components below 0.01 Hz. Although these fluctuations could be observed using NMR measurements, they could not be detected using inductive measurements [17].

Another limitation of the inductive measurement is that the pickup coil does not share the same volume as the NMR sample. To avoid electrical interference with the RF coil, the pickup coil is located on a larger cylinder concentric with the RF coil. As a result, spatial variations in the temporal field fluctuations will generate a correction field that does not exactly match the field fluctuation at the NMR coil. The pickup coil is also sensitive to a variety of small sources that do not affect the NMR resonance, including the electric field associated with the voltage required to drive current through the magnet and vibrations. Vibrations that slightly shift or rotate the pickup coil with respect to the magnet produce a change in flux through the coil without any change in magnetic field. It is therefore important to validate the pickup coil measurements with NMR measurements.

2.2. NMR measurements

The ultimate objective of this study is to improve the quality of NMR measurements by reducing the amplitude of temporal field fluctuations. For this reason it is useful to define a quantitative metric for determining the effect of temporal field fluctuations upon NMR measurements. One approach is to derive a metric that describes the effect of field fluctuations on the spectra of a single free-induction decay or spin echo. A disadvantage of this method is that the spectra of a single NMR response is dominated by the spatial inhomogeneity of the field, rather than the effect of the field fluctuations that occur during the duration of the recorded NMR response. A previous study noted that the effect of field fluctuations on the amplitude of a spin-echo response increases with the time-to-echo [5]. This result is not surprising as the phase of the spin-echo is determined by the integral of the field fluctuations over the time-to-echo interval. Here we use the standard deviation of spin echo phase which is a sensitive metric of temporal magnetic field fluctuations. This metric has a significant advantage in that its sensitivity is not limited by field homogeneity. Furthermore, it is a more appropriate measurement for many multidimensional experiments, and provides a direct measure of phase noise.

A train of spin echoes is generated by the pulse sequence $\pi/2 - T_E/2 - \pi - T_E/2 - acquire - T_D$, where the delay T_D between successive sequences is sufficiently large to neglect spin-lattice relaxation. In the absence of temporal magnetic field fluctuations, the real component of the spin echo signal is

$$s_r(t) = M_o \exp\left(\frac{-T_E}{T_2} + \frac{-|t - T_E|}{T_2^*}\right)\cos(\omega t + \phi), \tag{4}$$

and to simplify notation, we set the phase of the spectrometer receiver so that $\phi = 0$. The center of the $\pi/2$ pulse defines $t = 0$ and the time-to-echo, T_E, defines the center of the spin echo. In the presence of temporal magnetic field fluctuations, the phase ϕ becomes time dependent. At the center of the echo,

$$\phi(T_E) = \gamma \int_0^{T_E/2} B_f(p)dp - \gamma \int_{T_E/2}^{T_E} B_f(p)dp, \tag{5}$$

where γ is the gyromagnetic ratio [5]. The phase $\phi(T_E)$ vanishes when $B_f(t)$ is a constant, or when T_E exactly matches the fundamental period of a periodic $B_f(t)$, in other cases, the phase $\phi(T_E)$ varies from echo to echo. Note that as the time-to-echo parameter T_E increases, the sensitivity of the phase $\phi(T_E)$ to low frequency fluctuations in $B_f(t)$ will increase.

To measure the standard deviation of the spin echo phase $\phi(T_E)$, a series of N spin echo sequences $\pi/2 - T_E/2 - \pi - T_E/2 - acquire - T_D$ is acquired to provide N measurements $\phi_n(T_E)$. The standard deviation of these measurements is

$$\sigma_{SE}(T_E) = \sqrt{E\left\{\left(\phi_n(T_E) - E\{\phi_n(T_E)\}\right)^2\right\}}, \tag{6}$$

where the expectations are approximated by the average

$$E\{x\} = \frac{1}{N}\sum_{n=1}^{N} x_n. \tag{7}$$

The metric $\sigma_{SE}(T_E)$ is a positive semi-definite function of T_E, and vanishes when the phase $\phi_n(T_E)$ is the same for all spin echoes. Eq. (6) provides a way for both estimating $\sigma_{SE}(T_E)$ from experimental measurements and predicting its value given knowledge of $B_f(t)$.

Several factors must be considered when designing an NMR experiment to estimate $\sigma_{SE}(T_E)$. First, in resistive magnets, the temporal fluctuations and spatial inhomogeneity of the field broaden the linewidth, and so excitation of the entire line requires the use of short RF pulses. Second, in order to maximize the measurement SNR and to avoid generation of stimulated echoes, the time delay T_D between consecutive echoes is chosen much larger than the spin-lattice relaxation time T_1. Third, the number of repetitions must be chosen sufficiently large to reduce the variance of the estimate $\sigma_{SE}(T_E)$. Fourth, the maximum value of the time-to-echo parameter is chosen so that the phase measurement $\phi_n(T_E)$ lies in the interval $[-\pi, \pi]$. Larger values of T_E that cause the net phase measurement to sweep through $\pm\pi$ lead to phase ambiguity.

As an example of the effect of temporal magnetic field fluctuations on NMR measurements, Fig. 2 illustrates the spin echo response acquired in a superconducting magnet and the Keck resistive magnet, both operating at 7.1 T. The sample is a 1 mM $CuSO_4$ solution in a 5 mm NMR tube. A series of eighty spin echoes is generated by the pulse sequence $\pi/2 - T_E/2 - \pi - T_E/2 - acquire - T_D$, where the time-to-echo (T_E) is set to 5 ms. The time delay T_D is set to 1 s so that the effect of spin-lattice relaxation can be neglected.

In the superconducting magnet, the temporal magnetic field fluctuations are negligible over the duration of the experiment, and so the resulting spin echoes have the same phase, as shown in Fig. 2A. In stark contrast, the spin echoes acquired in the uncompensated Keck resistive magnet no longer align in time due to the presence of temporal magnetic field fluctuations, as shown in Fig. 2B. A comparison of Fig. 2A and B also shows that the spatial inhomogeneity of the resistive magnetic field significantly broadens the observed linewidth.

3. Feedback compensation

Temporal magnetic field fluctuations are attenuated using the feedback system represented in Fig. 3. The block diagram representation facilitates analysis using Laplace transform techniques. In addition to the transfer function $H_{int}(s)$ of the integrating preamplifier introduced in Section 2.1, we use the transfer functions

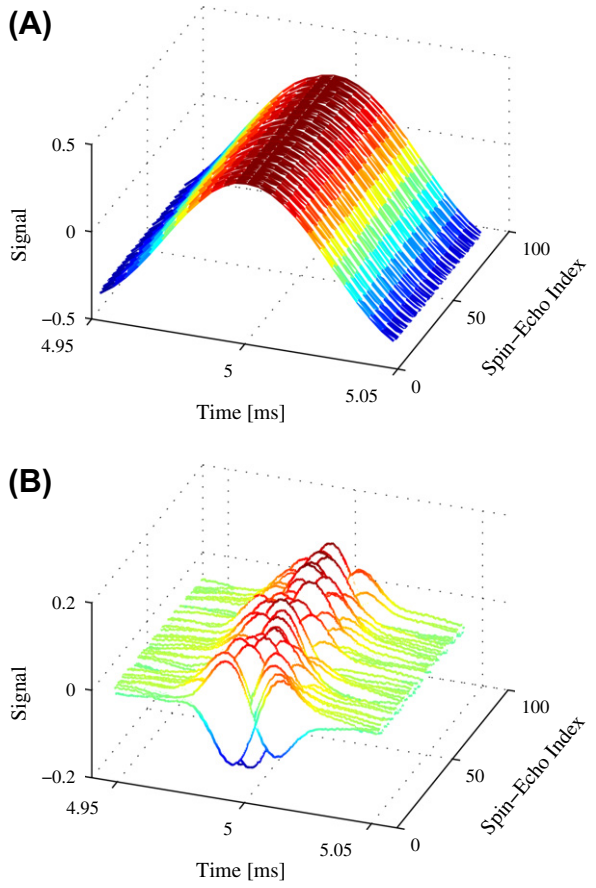

Fig. 2. Consecutive spin echo responses in a (A) 7.1 T superconducting magnet and the (B) Keck resistive magnet operating at 7.1 T.

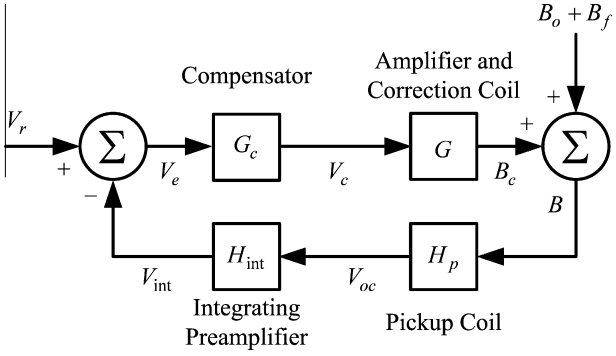

Fig. 3. Block diagram of the feedback control system.

$G_c(s)$, $G(s)$, and $H_p(s)$ to represent the compensator, the cascade combination of the amplifier and correction coil, and the pickup coil, respectively.

The magnetic field at the NMR sample is denoted as $B(t)$ and represents a superposition of the constant magnetic field B_0, the undesirable temporal fluctuations $B_f(t)$, and a correction field $B_c(t)$ generated by the closed-loop system. Ideally, the correction field cancels the magnetic fluctuations $B_f(t)$ so that the NMR sample experiences a constant magnetic field B_0.

From a control engineering viewpoint, the closed-loop system has a single output, $B(t)$, and two inputs. The disturbance input $B_f(t)$ represents the magnetic field fluctuations, and the reference input $v_r(t)$ represents the desired value of the integrating preamplifier output voltage $v_{int}(t)$ and, indirectly, the field $B(t)$. If a field sweep function were required, such as for a field frequency lock, it would be applied at the reference input. The output of the first summing junction, $v_e(t) = v_r(t) - v_{int}(t)$, represents the error signal that drives the compensator input. The compensator is designed so that the error signal is driven to zero, and correspondingly, the magnetic field within the pickup coil becomes constant.

Fig. 4 shows the relative placement of the pickup and correction coil with respect to the NMR sample tube. The pickup coil was wound on the glass VT insulator of a 5 mm solution NMR probe designed for the Keck magnet (Doty Scientific, Columbia, SC). The pickup coil is described in Section 2.1. The correction coil consisted of 73 turns of 3.2 mm wide adhesive copper tape. It was 285 mm in length, and wound on a fiberglass sleeve of outer diameter 44.2 mm that fit between the probe shield and magnet bore. The NMR probe was mounted from below the magnet, while the correction coil was mounted from above. The pickup and correction coils were centered around the NMR coil.

3.1. Design considerations

Two general objectives guide the compensator design. The first objective is to obtain a stable closed-loop system. If the system is dynamically unstable, the ensuing parasitic oscillations add to the undesirable effects of the field fluctuations $B_f(t)$. The second objective is to minimize the effect of the magnetic field fluctuations $B_f(t)$ on the field $B(t)$ seen by the NMR sample, or equivalently, minimize the amplitude of the error signal $v_e(t)$. The transfer function from the disturbance input, $B_f(t)$, to the error signal, $v_e(t)$, is

$$\frac{V_e(s)}{B_f(s)} = \frac{H_p(s)\, H_{int}(s)}{1 + G_c(s)\, G(s)\, H_p(s)\, H_{int}(s)}. \tag{8}$$

For the present analysis, we will consider the transfer functions $H_p(s)$, $H_{int}(s)$ and $G(s)$ to be fixed. On the other hand, the designer is free to select the compensator $G_c(s)$ so that the closed-loop system

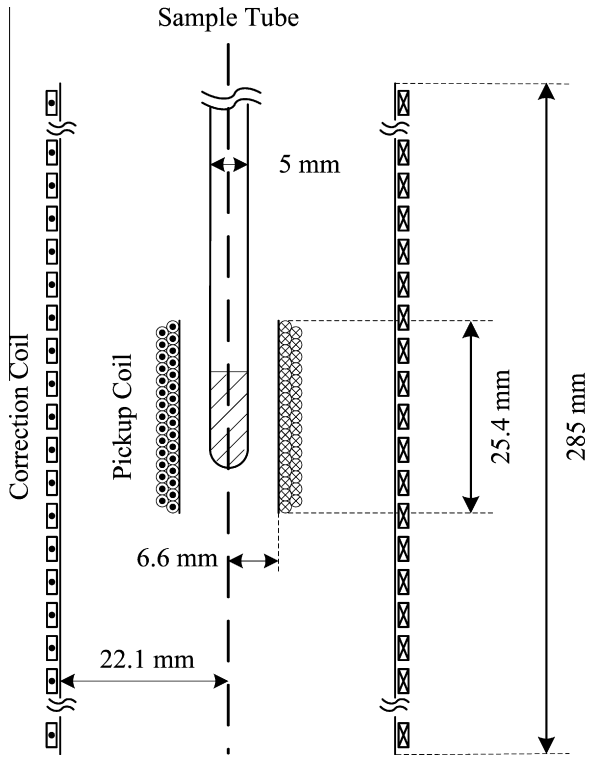

Fig. 4. Size and location of the pickup coil and correction coil with respect to the NMR sample.

is stable and the magnitude of the transfer function $V_e(s)/B_f(s)$ is minimized over a desired frequency range. The discussion in Section 2.2 reveals that as the RF pulse spacing increases, the lower frequency components of the magnetic field fluctuations have a greater effect on the phase of the NMR signals. Reducing the low frequency magnitude of the transfer function $V_e(s)/B_f(s)$ requires increasing the magnitude of the compensator $G_c(s)$ over the corresponding spectral range.

For simple proportional control, $G_c(s)$ would be set to a constant gain k_p. Increasing the value of the gain k_p decreases the magnitude of the transfer function $V_e(s)/B_f(s)$ in Eq. (8). However, depending on the pole and zero locations of the transfer functions $H_p(s)$, $H_{int}(s)$ and $G(s)$, there is a maximum value of k_p for which the closed-loop system is stable. In this case, the trade-off between closed-loop stability and disturbance rejection capability limits the ability to attenuate magnetic field fluctuations.

Nyquist stability theory provides a tool for determining whether or not a given compensator design leads to a stable closed-loop system [32]. In short, the closed-loop stability is guaranteed if the magnitude of the loop transfer function

$$\frac{V_e(s)}{V_{int}(s)} = G_c(s)\ G(s)\ H_p(s)\ H_{int}(s), \tag{9}$$

is less than 0 dB for frequencies above which the phase of the loop transfer function is less than $-180°$. The frequency at which the phase of the loop transfer function is $-180°$ defines the gain crossover frequency ω_{gc}. The gain margin Gm is defined as $1/G$, where G is the magnitude of the loop transfer function at ω_{gc}. In units of decibels, $Gm_{dB} = 20\log_{10}(Gm)$. The gain margin specifies the change in gain required to make the closed system unstable.

Systems with large gain margins have desirable transient response properties, such as small peak overshoots to abrupt changes in input variables, such as $B_f(t)$. A closed-loop system is stable for positive values of gain margin Gm_{dB}, and unstable for negative values of gain margin Gm_{dB}. An intuitive understanding of gain margin follows from considering Fig. 3. When the gain margin is negative, the loop transfer function gain is greater than unity at ω_{gc}. As a result, the frequency component of the error signal $v_e(t)$ at ω_{gc} is amplified. Because of the $-180°$ phase shift at the gain margin frequency and the inverting input at the summer, the feedback signal $v_{int}(t)$ adds constructively to the signal $v_e(t)$ at the compensator input, causing the closed-loop system to oscillate.

An understanding of Nyquist stability theory reveals that proportional control is a poor choice for designing a feedback system that reduces temporal magnetic field fluctuations. Increasing the proportional gain to reduce the magnetic field fluctuations decreases the gain margin, and hence the relative degree of stability of the closed-loop system. A better approach is to increase the low frequency gain of the compensator to reduce the effect of magnetic field fluctuations on the NMR signal, while rolling off the high frequency gain of the compensator to maintain a stable closed loop system with a positive gain margin.

Designing the compensator $G_c(s)$ using Nyquist stability theory requires knowledge of the open loop transfer function

$$\frac{V_{int}(s)}{V_c(s)} = G(s)\ H_p(s)\ H_i(s). \tag{10}$$

The transfer functions of the probe and integrating preamplifier are easily found from a first principle analysis. In contrast, the complexity of commercial power amplifiers and the magnetic coupling between the correction coil and its surrounding environment warrant the use of experimental data to estimate the transfer function $G(s)$. In the next subsection, standard system identification techniques are used to estimate the open loop transfer function $V_{int}(s)/V_c(s)$.

3.2. System identification

A two-step process provides an estimation of the open loop transfer $V_{int}(s)/V_c(s)$. In the first step, a DSA captures the magnitude and phase response of the open loop transfer function. The second step is to estimate a transfer function from the frequency response data using a curve-fitting algorithm that is available in most software packages supporting control system design and analysis.

The instrumentation configuration for the system identification experiments appears in Fig. 5. The DSA has a source and two inputs denoted by channel 1 and channel 2. The source provides a sinusoidal excitation for the system identification experiment and is connected to the input of the power amplifier and channel 1. The output of the integrating preamplifier connects to channel 2, and the DSA automatically adjusts the excitation amplitude to maintain a good measurement SNR at channel 2. The DSA determines the amplitude ratio and phase difference of the sinusoidal signals appearing at channels 1 and 2 to determine the magnitude $|G(\jmath\omega_k)|$ and phase $\angle G(j\omega_k)$ of the open loop transfer function at a discrete number of frequencies ω_k over a spectral range specified by the user.

Assuming that the open-loop system is linear time-invariant, the estimate of its frequency response function has the form

$$\widehat{G}(j\omega) = \frac{V_{int}(j\omega)}{V_c(j\omega)} = \frac{b_m(j\omega)^m + b_{m-1}(j\omega)^{m-1} + \cdots + b_0}{(j\omega)^n + a_{n-1}(j\omega)^{n-1} + \cdots + a_0}. \tag{11}$$

The goal of system identification is to determine the parameters m, n, b_j, and a_j so that the estimated frequency response function $\widehat{G}(j\omega)$ is a good approximation of the true frequency response function $G(j\omega)$ in the sense of minimizing the cost function

$$J(a_j, b_j; n, m) = \sum_{k=1}^{N} \left| G(j\omega_k) - \widehat{G}(j\omega_k) \right|^2. \tag{12}$$

As the quantity $\left|G(j\omega_k) - \widehat{G}(j\omega_k)\right|^2$ represents squared magnitude of the error between the true and estimated frequency response at a particular frequency ω_k, the performance index J is represents the sum of the squared magnitude errors at a sequence of frequencies $\omega_1, \omega_2, \ldots \omega_N$.

By specifying the number of poles, n, and the number of zeros, m, a complex-curve fitting algorithm provides a least-squares estimate of the coefficients a_j and b_j and the corresponding value of the cost function $J(a_j, b_j; n, m)$ [33]. In brief, a necessary condition for the parameter set $\{a_1, \ldots, a_n, b_1, \ldots b_m\}$ to minimize J is that $\partial J/\partial a_1 = \ldots \partial J/\partial a_n = \partial J/\partial b_1 = \ldots \partial J/\partial b_m = 0$. These equalities provide $n + m$ equations that can be solved for the $n + m$ unknowns $\{a_1, \ldots, a_n, b_1, \ldots b_m\}$. For a range of values of n and m, the parameter set that minimizes the cost function is determined by solving a set of $n + m$ equations, and the corresponding value of the cost

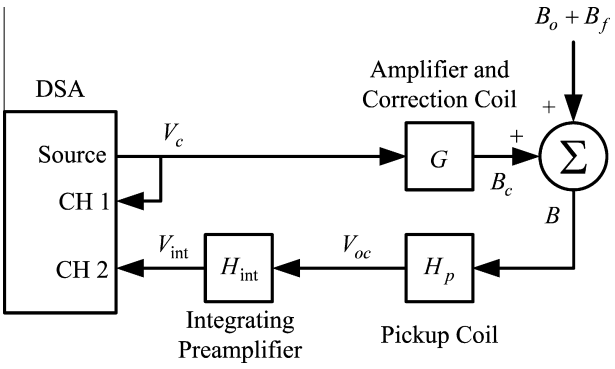

Fig. 5. Experimental setup for system identification.

function J is determined. The pair (m,n) that minimizes J and the corresponding coefficients a_j and b_j specify the estimated transfer function.

For the Keck resistive magnet, choosing six poles and three zeros minimizes the cost function J. Fig. 6 shows the frequency response obtained from the DSA measurements and the estimated frequency response function. The blue curve shows the measured frequency response for the Keck resistive magnet operating at 7.1 T, while the dashed red curve shows the identified frequency response function. The ripple and the bump at 60 Hz are artifacts from the magnetic field fluctuations. To determine if the frequency response function is affected by the field strength of the magnet, we also measured the frequency response for the Keck resistive magnet operating at 0 T. The green dashdot curve shows that the measured frequency response at 0 T is nearly indistinguishable from the identified frequency response function shown by the dashed red curve.

3.3. PLL-IMP compensator design

The gain margin of the estimated and measured open-loop transfer functions in Fig. 6 is approximately 6 dB. Allowing for a 2 dB gain margin, the largest possible proportional control gain is 4 dB, or equivalently, a factor of 1.6. Setting $G_c(s) = 1.6$, the loop transfer function in Eq. (9) provides a nearly flat gain from 24 dB at 0.1 Hz, to the 3 dB corner frequency at 1 kHz. An attempt to further reduce the magnetic field fluctuations by increasing the proportional gain will produce an unstable closed loop system.

In order to increase the low frequency gain of the loop transfer function while maintaining the stability of the closed loop system, a phase-lag controller is employed. This controller provides a large gain at low frequencies to reduce the effect of disturbances and rolls off the high frequency gain to maintain a positive gain margin. Following standard design techniques [32], we obtain a phase-lag controller with the transfer function representation

$$G_{lag}(s) = K\frac{\frac{s}{2\pi\cdot 2370}+1}{\frac{s}{2\pi\cdot 16}+1}, \tag{13}$$

where the parameter K represents the DC gain of the compensator. At frequencies below 16 Hz, the transfer function $G_{lag}(s)$ has gain K. For frequencies between 16 Hz and 2370 Hz, the gain decreases by 20 dB/dec. For frequencies above 2370 Hz, the gain levels off to $16K/2370$. This controller increases the DC gain by 67 dB with respect to the high frequency gain. Setting $G_c(s) = G_{lag}(s)$ with $K = 1$ results in a gain margin of 38 dB. That is, the closed-loop system is stable for any DC gain K lower than 38 dB, or equivalently, $K \leqslant 80$.

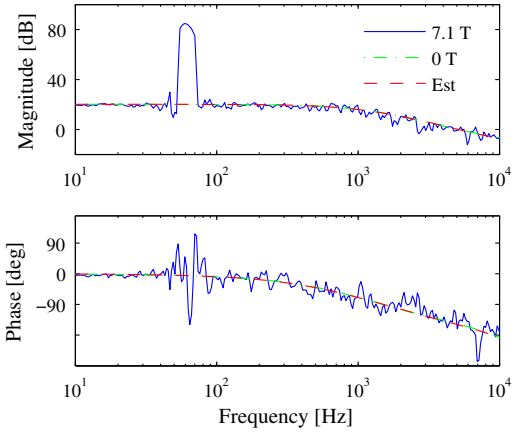

Fig. 6. Measured and estimated frequency response of the open-loop transfer function for the Keck magnet system.

In practice, the DC offset of the integrating preamplifier limits the maximum DC gain of the compensator. Although the integrating preamplifier is not a pure integrator, it has a large gain at frequencies near DC. Small DC offsets at the input stage of the integrating preamplifier lead to saturation of the power amplifier. The presence of the DC offset reduced the maximum practical DC gain from 38 dB to 25 dB, thereby reducing the effectiveness of the phase-lag controller.

A phase-lead-lag control design overcomes this limitation. Unlike a conventional phase-lead-lag controller, in which the phase-lead component increases the high frequency loop gain without compromising closed-loop stability, the phase-lead-lag design presented here utilizes a phase-lead component to roll-off the low frequency gain. The phase-lead component reduces the DC gain of the overall compensator below the maximum value set by the DC offset of the integrating preamplifier. Simultaneously, it achieves the maximum possible loop gain afforded by the phase-lag component above the frequency set by the phase-lead pole. The transfer function representation of the phase lead component is

$$G_{lead}(s) = \frac{\frac{s}{2\pi\cdot 0.016}+1}{\frac{s}{2\pi\cdot 0.16}+1}. \tag{14}$$

This compensator provides unity gain at frequencies below 16 mHz. Between 16 mHz and 160 mHz, the gain rises at 20 dB per decade and then levels off to 20 dB at higher frequencies. When included in the composite controller, the phase-lead component provides 20 dB more gain than just the phase-lag controller for frequencies above 160 mHz.

A series cascade of the phase-lag and phase-lead controllers result in a phase-lead-lag controller with the transfer function

$$G_c(s) = G_{lag}(s)G_{lead}(s) = \left(K\frac{\frac{s}{2\pi\cdot 2370}+1}{\frac{s}{2\pi\cdot 16}+1}\right)\left(\frac{\frac{s}{2\pi\cdot 0.016}+1}{\frac{s}{2\pi\cdot 0.16}+1}\right). \tag{15}$$

With the DC gain K set to unity, the gain margin of the loop transfer function is 18.3 dB. The maximum value of K that yields a stable closed-loop system is 18.3 dB, or equivalently, a factor of 8. We choose K as 6, which provides a gain margin of 2.24 dB. Between 0.3 Hz and 10 Hz, this choice of DC gain yields a loop transfer function gain of 54 dB.

By applying a concept known as the internal model principle (IMP), we can further attenuate harmonic components of the magnetic field fluctuations. In general, a disturbance within a given frequency band can be attenuated by increasing the gain of the loop transfer function over that band. As an example, proportional plus integral controllers eliminate the effect of constant disturbances because they provide a large loop gain at low frequencies. This gain results from placing the controller pole at the origin of the s-plane, which corresponds to the location of the DC disturbance. The internal model principle extends this technique to time-varying disturbances [34,35]. In particular, the controller poles are chosen to provide high gain at the spectral location of the disturbance. These compensator poles appear as zeros located at the disturbance frequencies in the transfer function from the disturbance input to the closed-loop output.

In order to cancel a sinusoid of a given frequency, the poles of the IMP controller must correspond to the poles of the sinusoidal disturbance. The Laplace transform of the n^{th} harmonic of the power supply ripple has the form

$$\mathcal{L}\{\sin(n\omega_0 t)\cdot u(t)\} = \frac{n\omega_0}{s^2+(n\omega_0)^2}, \tag{16}$$

where $\omega_0 = 2\pi\cdot 60$ Hz, n is a positive integer, and $u(t)$ is the unit step function. Applying the internal model principle, the compensator transfer function must contain poles identical to those in Eq. (16). However, as these poles lie on the $j\omega$ axis, the resulting loop

transfer function is marginally stable. To obtain a stable closed loop transfer function, the compensator poles are shifted slightly into the left-half plane. To avoid altering the shape of the loop transfer function obtained using the phase-lead-lag control design, a pair of additional complex conjugate zeros are placed to the left of the complex conjugate poles. For a single harmonic $n\omega_0$, the compensator includes a pair of complex poles and zeros, and is represented as

$$G_n(s) = \frac{\beta_n^2 + (n\omega_0)^2}{\alpha_n^2 + (n\omega_0)^2} \frac{(s+\alpha_n)^2 + (n\omega_0)^2}{(s+\beta_n)^2 + (n\omega_0)^2}, \tag{17}$$

where α_n and β_n are the real parts of the complex zeros and poles respectively. The leading factor forces the transfer function to have unity DC gain.

The selection of α_n and β_n involves several tradeoffs. In order to provide a large loop gain at a disturbance frequency $n\omega_0$, it is desirable to have β_n as small as possible so that the compensator complex pole pair is located adjacent to the imaginary axis. As the controller is implemented with a dedicated digital signal processor with finite register lengths, β_n must be large enough so that rounding errors do not place the closed-loop poles outside the stability boundary.

Choosing the distance $\alpha_n - \beta_n$ between a given pole-zero pair along the real axis presents a design trade-off between the disturbance rejection performance and the relative degree of closed-loop stability. As the distance $\alpha_n - \beta_n$ increases, there is a desirable increase in the magnitude and bandwidth of the peak in the loop transfer function located at the disturbance frequency $n\omega_0$. However, increasing the distance also reduces the gain margin by decreasing the gain crossover frequency.

In our system, the maximum number of harmonics that can be attenuated using the internal model principle is limited by the computational speed of the digital signal processing (DSP) system used to implement the compensator $G_c(s)$. A minimum sample period of 20 μs allowed us to include an IMP component that attenuates the four largest amplitude harmonics which are located at 60 Hz, 120 Hz, 180 Hz, and 720 Hz. The transfer function of the IMP component was set to be

$$G_{IMP}(s) = \prod_{n=1,2,3,12} G_n(s), \tag{18}$$

where $\alpha_n = 100$ and $\beta_n = 0.1$ for each n. Cascading the IMP compensator in Eq. (18) with the phase-lead-lag compensator in Eq. (15) results in the PLL-IMP compensator with transfer function

$$G_c(s) = G_{lag}(s)G_{lead}(s)G_{IMP}(s). \tag{19}$$

Fig. 7 shows the frequency response of the loop transfer function in Eq. (9) with phase-lead-lag-IMP compensation. As this compensator inherits the phase-lead-lag controller, its frequency response is close to that of the phase-lead-lag system, except at the frequencies where the complex pole-zero pairs are located. Near 60 Hz, 120 Hz, 180 Hz and 720 Hz, the magnitude response has significantly higher gain. For example, the presence of the IMP component at 60 Hz increases the loop gain from 54 dB to 100 dB. Once the feedback loop is closed, the magnitude of the transfer function between the disturbance input $B_f(t)$ and the integrating preamplifier output $v_{int}(t)$ admits notches at 60 Hz, 120 Hz, 180 Hz and 720 Hz.

3.4. Controller implementation

Because the PLL-IMP compensator $G_c(s)$ is a 10th-order system, implementing it with an analog circuit is neither convenient nor practical. Instead, we approximate the continuous time compensator $G_c(s)$ using the sampled-data system of Fig. 8, where the sample rate $1/T$ is significantly larger than the bandwidth of the transfer

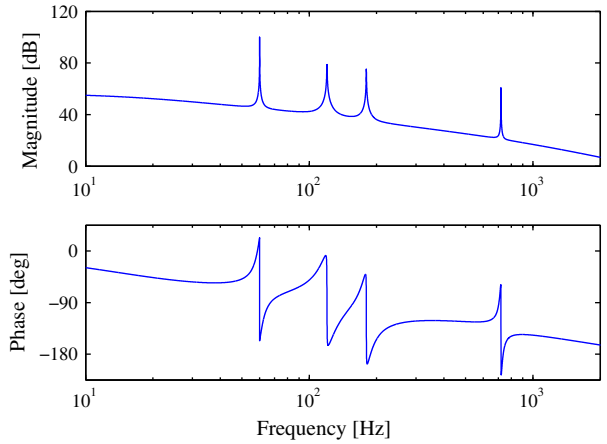

Fig. 7. The loop transfer function $V_e(s)/V_{int}(s)$ using phase-lead-lag-IMP compensation.

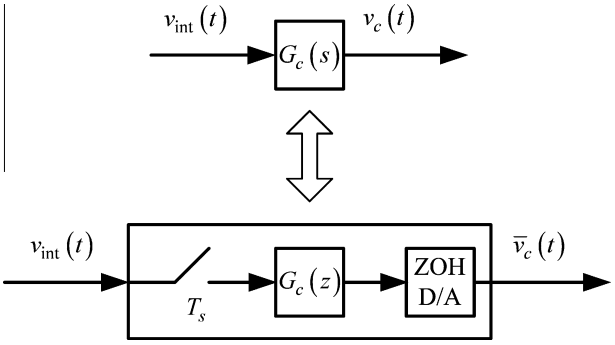

Fig. 8. Realization of the analog controller $G_c(s)$ using a sampled-data system.

function $G_c(s)$. Another advantage of sampled-data systems is that they allow rapid implementation of changes in control design. Replacing an analog control design may require extensive circuit modifications, while sampled-data controllers are easily changed through software modification.

The transfer function $G(z)$ of the digital controller is the zero-order hold equivalent of the analog compensator $G_c(s)$, and is calculated as

$$G_c(z) = \frac{z-1}{z} \mathcal{Z}\left[\frac{G_c(s)}{s}\right]_{e^{sT_s}=z}, \tag{20}$$

where $T_s = 20$ μs is the sample period [36]. The output $\bar{v}_c(t)$ is a staircase waveform and exactly matches the output $v_c(t)$ of the analog compensator at the sample instants $t = kT_s$.

Sampled-data systems quantize the analog waveform not only in time, but also in amplitude, as the sampled values are stored in finite-length registers. Our digital signal processing system utilizes 16-bit analog-to-digital (A/D) and digital-to-analog (D/A) converters. To use the maximum dynamic range of the A/D converter, the gain of the integrating preamplifier is set as large as possible without exceeding the A/D input limit.

3.5. Comparison of compensator designs

The flux regulation systems based on proportional control and the PLL-IMP design were evaluated using the Keck resistive magnet operating at 7.1 T. Fig. 9 illustrates the magnitude spectra of the field fluctuations detected by the pickup coil with and without flux regulation afforded by both control designs discussed in Section 3.

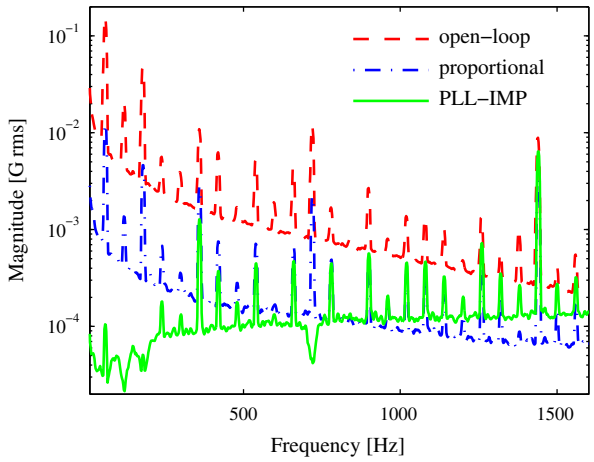

Fig. 9. Magnitude spectra of the temporal magnetic field fluctuations in the Keck resistive magnet operating at 7.1 T, with and without feedback compensation.

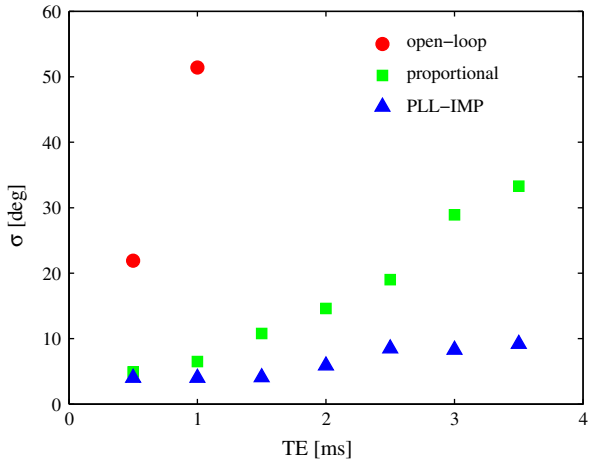

Fig. 10. Measured standard deviation of spin-echo phase for the Keck resistive magnet at 7.1 T field with, and without, feedback compensation.

Without regulation, the dashed red curve shows that the 60 Hz component has a magnitude of 160 mG rms.

Proportional compensation attenuates both the harmonic peaks and the background noise by the same amount, as shown by the dashdot blue[1] curve in Fig. 9. The proportional gain is set to achieve the greatest reduction in magnetic field fluctuations while maintaining closed-loop stability. The 60 Hz component is reduced by 24 dB to 10 mG rms. A similar attenuation factor at higher harmonics is possible because the magnitude response of the proportional control system is frequency independent.

The solid green curve in Fig. 9 shows that the PLL-IMP compensator yields a significantly greater reduction in the low frequency harmonics. The PLL-IMP design reduces the magnitude of the 60 Hz component by 64 dB to 0.1 mG rms, or equivalently, 0.02 ppm rms. In order to maintain closed-loop stability, the gain of the PLL-IMP compensator rolls off with increasing frequency. As a result, the proportional controller achieves a marginally greater reduction in the magnitude of harmonic components located above 800 Hz. For example, the magnitudes of the harmonic component located at 780 Hz for the PLL-IMP and proportional control design are 0.45 mG rms and 0.49 mG rms, respectively. In contrast, the magnitudes of the harmonic component located at 960 Hz for the PLL-IMP and proportional control design are 0.21 mG rms and 0.18 mG rms, respectively.

Fig. 10 shows the results obtained from spin echo phase measurements using the Keck resistive magnet operating at 7.1 T and a 1 mM solution of $CuSO_4$. The standard deviation of spin echo phase is plotted as a function of echo time T_E for the same three cases shown in Fig. 9. The value of σ_{SE} is estimated from experimental data using the spin-echo pulse sequence described in Section 2.2. Red circles show the results obtained without compensating for field fluctuations, while the green squares and blue triangles show the results obtained with the proportional and PLL-IMP control designs, respectively. In each case, the standard deviation of spin echo phase increases with the time-to-echo. As feedback compensation significantly reduces the amplitude of the magnetic field fluctuations, it is not surprising the standard deviation of spin echo phase is also reduced. For a time-to-echo of 1 ms, the metric σ_{SE} is 51° in the absence of a feedback compensation. In contrast, both proportional and PLL-IMP compensation reduces σ_{SE} to about 6°. As the value of the time-to-echo increases, the PLL-IMP compensator achieves a greater reduction in the metric σ_{SE} than does

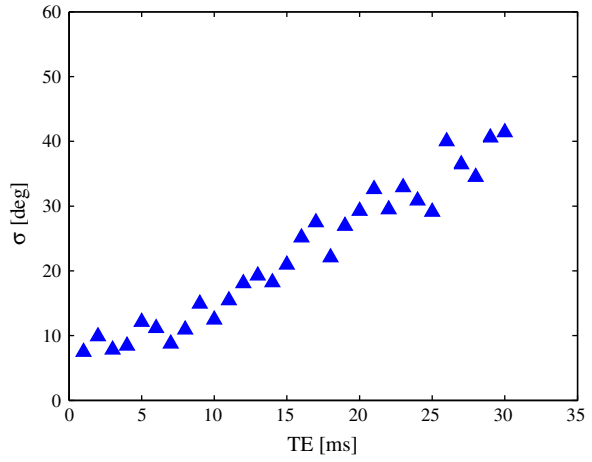

Fig. 11. Measured standard deviation of spin-echo phase for the Keck magnet at 7.1 T field with PLL-IMP compensation.

proportional compensation. For example, when the time-to-echo is set to 3.5 ms, σ_{SE} is about 33° using proportional control, while the PLL-IMP compensator reduces σ_{SE} to approximately 9°.

To further assess the performance of the sampled-data PLL-IMP compensator, we repeated the spin echo experiment in Section 2.2 for substantially longer values of the time-to-echo parameter T_E. The data in Fig. 11 shows that σ_{SE} continues to increase with T_E. To gauge the effectiveness of the PLL-IMP compensator, note that the value of σ_{SE} measured under PLL-IMP compensation when T_E is 30 ms is approximately 41°, which is smaller than the value of σ_{SE} for the uncompensated magnet system when T_E is 1 ms.

In addition to comparing the performance of the proportional and PLL-IMP compensator designs using the metric σ_{SE}, it also useful to plot individual echoes as in Fig. 2. Using a sample of 1 mM solution of $CuSO_4$, one hundred spin echoes were consecutively acquired with the pulse sequence $\pi/2 - T_E/2 - \pi - T_E/2 - acquire - T_D$, where the time-to-echo (T_E) is set to 7 ms and the time delay T_D is 1 s. Fig. 12A and B shows every tenth echo acquired for the proportional and PLL-IMP controller, respectively. The PLL-IMP provides an obvious advantage in phase regularity over the proportional control. For the case of the PLL-IMP compensation, the value of σ_{SE} is 8.8°, while for proportional control, we cannot provide a value for σ_{SE} because the large phase difference between consecu-

[1] For interpretation of color in Figs. 1, 2, 6, 7 and 9–12, the reader is referred to the web version of this article.

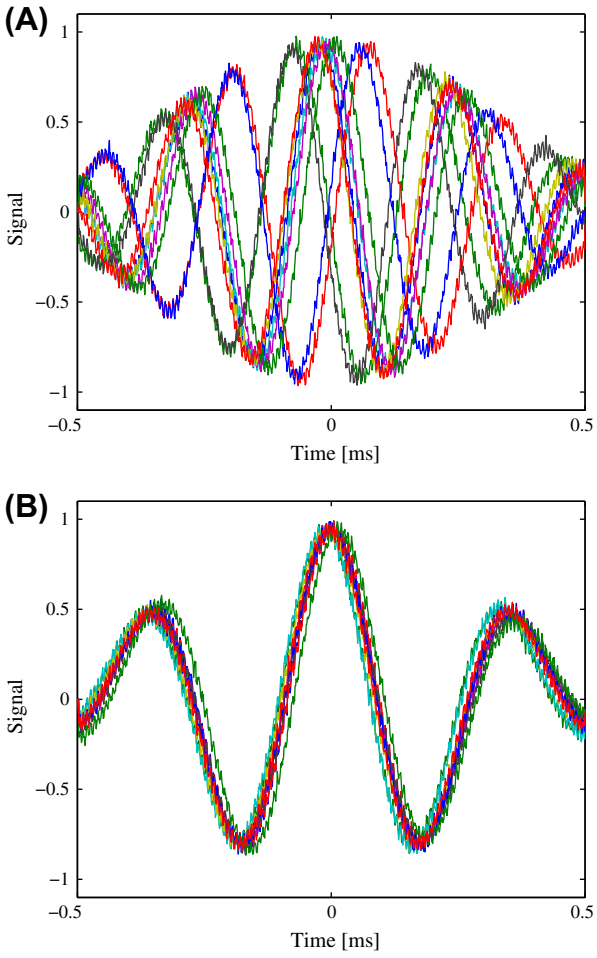

Fig. 12. Spin echo responses for a T_E value of 7 ms in the Keck resistive magnet operating at 7.1 T using (A) proportional and (B) PLL-IMP flux regulation.

tive echoes leads to phase ambiguity. In specific, we cannot determine if the phase variation is θ or $\theta - 2\pi$.

4. Discussion

The present technology for high-field superconductive NMR magnets, based on low-temperature superconductors, has an upper bound on magnetic field strength of slightly higher than 21 T [37]. Higher field strengths appear to be possible with conductors made from high-temperature superconductor materials, but such magnets are some years in the future [38]. Resistive and hybrid superconducting/resistive magnets can provide fields up to at least 45 T using current technology, although they require an external power supply and water cooling system. High resolution NMR in these magnets requires overcoming the spatial inhomogeneity and temporal fluctuations that are characteristic of resistive magnets. Earlier investigators achieved reductions in temporal magnetic field fluctuations using analog feedback control systems. This paper has built upon their work in two ways. First, shaping the frequency response of the compensator yields significantly greater reductions in magnetic field fluctuations in comparison to proportional compensation. Second, the use of a sampled-data controller eliminates the complexity of implementing an analog compensator with multiple poles and zeros.

A flux regulator using proportional compensation has a single adjustable gain parameter whose selection requires a compromise between reducing the amplitude of magnetic field fluctuations and maintaining the stability of the closed-loop system. The PLL-IMP compensator described above provides significantly greater attenuation by increasing the loop gain at frequencies corresponding to disturbance components. For example, proportional compensation reduces the amplitude of the 60 Hz magnetic fluctuation in the Keck resistive magnet by 24 dB. In comparison, the PLL-IMP controller further reduces the amplitude of this component by 40 dB.

The PLL-IMP compensator developed for the Keck resistive magnet has a transfer function with ten poles and ten zeros. Implementing such a high-order transfer function with an analog circuit is feasible but not desirable. An analog circuit requires an impractical number of adjustable components in order to place the poles and zeros of the IMP compensator at their desired locations. Furthermore, attenuating additional power supply harmonics or making other changes to the control design would require extensive circuit modifications. A dedicated signal processing system reduces development time and cost because the controller is specified in block diagram format using a graphical user interface.

The 1/f noise in the inductive field measurements limits the ability of the flux regulator to attenuate low frequency field fluctuations. An effort to reduce 1/f noise by redesigning the integrating preamplifier is underway. Although this work will improve the inductive measurement SNR for low frequencies, amplifier noise will always mask the magnetic field fluctuations below some frequency limit. In order to sense magnetic field fluctuations below this limit, a field-frequency lock is necessary.

Acknowledgments

This work was supported by the US National Science Foundation and the State of Florida through NSF Cooperative Agreement DMR-0654118. This work was also partially supported by NSF through DMR-0412169. The authors would like to express appreciation to Mark D. Bird, Timothy A. Cross, James A. Powell, Peter L. Gor'kov, Zhehong Gan, Steve A. Suddarth and many others at the NHMFL who have contributed to the development of high resolution NMR in resistive magnets.

References

[1] Z. Gan, P.L. Gor'kov, T.A. Cross, A. Samoson, D. Massiot, Seeking higher resolution and sensitivity for NMR of quadrupolar nuclei at ultrahigh magnetic fields, J. Am. Chem. Soc. 124 (2002) 5634–5635.
[2] Y.-Y. Lin, S. Ahn, N. Murali, W.W. Brey, C.R. Bowers, W.S. Warren, High-resolution, >1 GHz NMR in unstable magnetic fields, Phys. Rev. Lett. 85 (2000) 3732–3735.
[3] L. Peng, Z.Y. Zheng, Y.Q. Huang, Z.M. Zhang, S.H. Cai, Z. Chen, High-resolution NMR spectra in inhomogeneous and unstable fields via the three-pulse method, Mol. Phys. 108 (2010) 1869–1875.
[4] J.-H. Cho, S. Ahn, C. Lee, K.S. Hong, K.-C. Chung, S.-K. Chang, C. Cheong, W.S. Warren, Magnetic resonance microscopic imaging based on high-order intermolecular multiple-quantum coherences, Magn. Reson. Imag. 22 (2007) 1407–1412.
[5] E.E. Sigmund, E.S. Calder, G.W. Thomas, V.F. Mitrovic, H.N. Bachman, W.P. Halperin, P.L. Kuhns, A.P. Reyes, NMR phase noise in Bitter magnets, J. Magn. Reson. 148 (2001) 309–313.
[6] B. Shapira, K.K. Shetty, W.W. Brey, Z.H. Gan, L. Frydman, Single-scan 2D NMR spectroscopy on a 25 T Bitter magnet, Chem. Phys. Lett. 44 (2007) 478–482.
[7] S. Hong, M.B. Field, J.A. Parrell, Y. Zhang, Latest improvements of current carrying capability of niobium tin and its magnet applications, IEEE Trans. Appl. Supercond. 16 (2006) 1146–1151.
[8] J. Bascuñán, W. Kim, S. Hahn, E.S. Bobrov, H. Lee, Y. Iwasa, An LTS/HTS magnet operated in the range of 600–700 MHz, IEEE Trans. Appl. Supercond. 17 (2007) 1446–1449.
[9] Y. Yanagisawa, H. Nakagome, K. Tennmei, M. Hamada, M. Yoshikawa, A. Otsuka, M. Hosono, T. Kiyoshi, M. Takahashi, T. Yamazaki, H. Maeda, Operation of a 500 MHz high temperature superconducting NMR, towards an NMR spectrometer operating beyond 1 GHz, J. Magn. Reson. 203 (2010) 274–282.
[10] M.B. Kozlov, J. Haase, C. Baumann, A.G. Webb, 56 T 1H NMR at 2.4 GHz in a pulsed high-field magnet, Solid State Nucl. Magn. Reson. 28 (2005) 64–67.
[11] J.R. Miller, The NHMFL 45-T hybrid magnet system: past, present, and future, IEEE Trans. Appl. Supercond. 13 (2003) 1385–1390.

[12] P.J.M. van Bentum, J.C. Maan, J.W.M. van Os, A.P.M. Kentgens, Strategies for solid-state NMR in high-field Bitter and hybrid magnets, Chem. Phys. Lett. 376 (2003) 338–345.
[13] J.R. Miller, M.D. Bird, A new series-connected hybrid magnet system for the National High Magnetic Field Laboratory, IEEE Trans. Appl. Supercond. 14 (2004) 1283–1286.
[14] A.B. Oliva, M.D. Bird, S.T. Bole, K.R. Cantrell, A.V. Gavrilin, C.A. Luongo, I.R. Dixon, K. Han, J. Lu, G.E. Miller, P.D. Noyes, T.A. Painter, J. Toth, H.W. Weijers, R.P. Walsh, Y. Zhai, Development of the superconducting outserts for the series-connected-hybrid program at the National High Magnetic Field Laboratory, IEEE Trans. Appl. Supercond. 18 (2008) 529–535.
[15] T.A. Painter, M.D. Bird, S.T. Bole, A.J. Trowell, K.K. Shetty, W.W. Brey, Resistive shims for high-field resistive and hybrid magnets, IEEE Trans. Appl. Supercond. 18 (2008) 1334–1337.
[16] H.J. Boenig, J.A. Ferner, F. Bogdan, R.S. Rumrill, G.C. Morris, Design and operation of a 40-MW highly stabilized power supply, IEEE Trans. Ind. Appl. 32 (1996) 1146–1157.
[17] V. Soghomonian, M. Sabo, A. Powell, P. Murphy, R. Rosanske, T.A. Cross, H.J. Schneider-Muntau, Identification and minimization of sources of temporal instabilities in high field (>23 T) resistive magnets, Rev. Sci. Instrum. 71 (2000) 2883–2889.
[18] J. Bechhoefer, Feedback for physicists: a tutorial essay on control, Rev. Mod. Phys. 77 (2005) 783–836.
[19] E.S. Meyer, I.F. Silvera, B.L. Brandt, Eddy current shielding and heating: reduction of dissipation for very low-temperature experiments in the presence of magnetic field ripple, Rev. Sci. Instrum. 60 (1989) 2964–2968.
[20] E.E. Sigmund, V.F. Mitrovic, E.S. Calder, G.W. Thomas, H.N. Bachman, W.P. Halperin, P.L. Kuhns, A.P. Reyes, Inductive shielding of NMR phase noise, J. Magn. Reson. 159 (2002) 190–194.
[21] G.A. Morris, H. Barjat, T.J. Horne, Reference deconvolution methods, Prog. Nucl. Magn. Reson. Spectrosc. 31 (1997) 197–257.
[22] T. Iijima, K. Takegoshi, K. Hashi, T. Fujito, T. Shimizu, High-resolution NMR with resistive and hybrid magnets: deconvolution using a field-fluctuation signal, J. Magn. Reson. 184 (2007) 258–262.
[23] T. Iijima, K. Takegoshi, Compensation of effect of field instability by reference deconvolution with phase reconstruction, J. Magn. Reson. 191 (2008) 128–134.
[24] Z. Gan, H.T. Kwak, M. Bird, T.A. Cross, P.L. Gor'kov, W.W. Brey, K.K. Shetty, High-field NMR using resistive and hybrid magnets, J. Magn. Reson. 191 (2008) 135–140.
[25] P. Pelupessy, E. Rennella, G. Bodenhausen, High-resolution NMR in magnetic fields with unknown spatiotemporal variations, Science 324 (2009) 1693–1697.
[26] H. Primas, H.H. Gunthard, Field stabilizer for high-resolution nuclear magnetic resonance, Rev. Sci. Instrum. 28 (1957) 510–514.
[27] H.H. Gunthard, Magnetic Field Stabilizer, 1958, US Patent 2,979,641.
[28] A.M. Gottlieb, V.C. Srivastava, P. Heller, L.G. Rubin, A tunable NMR spectrometer for the vhf-uhf Range, Rev. Sci. Instrum. 43 (1972) 676–680.
[29] M.E. Packard, A proton-controlled magnetic field regulator, Rev. Sci. Instrum. 19 (1948) 435–439.
[30] D.I. Hoult, R.E. Richards, P. Styles, A novel field-frequency lock for a superconducting spectrometer, J. Magn. Reson. 30 (1978) 351–365.
[31] M.D. Bird, Z. Gan, Low resolution NMR magnets in the 23 to 35 T range at the NHMFL, IEEE Trans. Appl. Supercond. 12 (2002) 447–451.
[32] G. Franklin, J.D. Powell, A. Emami-Naeini, Feedback Control of Dynamic Systems, Addison-Wesley, 2005.
[33] E.C. Levy, Complex-curve fitting, IRE Trans. Autom. Cont. 4 (1959) 37–44.
[34] B.A. Francis, The internal model principle of control theory, Automatica 12 (1976) 457–465.
[35] V. Kucera, Disturbance rejection: a polynomial approach, IEEE Trans. Autom. Cont. 28 (1983) 508–511.
[36] C.L. Phillips, Digital Control System Analysis and Design, Prentice Hall, 1995.
[37] I.R. Dixon, W.D. Markiewicz, W.W. Brey, K.K. Shetty, Performance of the ultra wide bore 900 MHz NMR magnet at the National High Magnetic Field Laboratory, IEEE Trans. Appl. Supercond. 15 (2005) 1334–1337.
[38] W.D. Markiewicz, J.R. Miller, J. Schwartz, U.P. Trociewitz, H.W. Weijers, Perspective on a superconducting 30 T/1.3 GHz NMR spectrometer magnet, IEEE Trans. Appl. Supercond. 16 (2006) 1523–1526.